# Model Predictive Control of a Heat Pump System Integrated with PVT Collectors and Ice Storage

**Daler Khamidov[1], Bruno B. Bampi[1], Lilli Frison[1], Björn Nienborg[1]**

[1] Fraunhofer Institute for Solar Energy Systems (ISE), Freiburg (Germany)

## Abstract

This paper focuses on optimizing a building heating system consisting of a heat pump, photovoltaic collectors (PVT), an ice storage tank, and a buffer tank. The aim is to assess the potential of using Mixed-Integer Nonlinear Model Predictive Control (MI-NMPC) in a novel heat pump system with dual heat sources—PVT collectors and ice storage, along with buffer storage. The paper investigates dynamic interactions, algorithm development, and performance evaluation, emphasizing energy efficiency, cost-effectiveness, and demand response. We find that control-oriented dynamic simulation accurately captures the system's behavior. The application of NMPC in this context highlights its potential for advanced control strategies in hybrid (switched) energy systems. The simulation results demonstrate the improved performance of the system using the MI-NMPC strategy compared to a reference Rule-Based Control (RBC) strategy. This improvement is reflected in a 17.4% reduction in electricity costs over the heating season and a 15.4% decrease in net costs, including revenue from selling excess energy to the grid. In addition, the MI-NMPC strategy increases the self-consumption rate of the generated PV power to 38.2%, further improving the economic and energy efficiency of the system. The application of MI-NMPC in this context underscores its potential for advanced control strategies in hybrid energy systems, particularly in multi-source heat pump systems.

*Keywords: Multi-Source Heat Pump, Ice Storage, Mixed-Integer NMPC, PVT, Control-oriented modelling.*

## 1. Introduction

To achieve a sustainable future, it is essential to address the limitations of finite resources, especially fossil fuels. Integrating renewable energy sources into the building sector is a critical part of this transition. Today, buildings account for approximately 30 percent of global final energy consumption and 26 percent of global energy emissions (International Energy Agency, 20/23). About 80 percent of households in Germany still rely on traditional heating systems based on fossil fuels (Bundesverband der Deutschen Heizung- und Warmwasserindustrie, 20/24). Modernization efforts have already helped avoid about 3 million tons of CO2 emissions by 2023 (Umweltbundesamt, 2023). Achieving greenhouse gas neutrality by 2045 and the interim goal of a 65 percent reduction in emissions by 2030 will require a shift to cleaner technologies such as heat pumps. Optimizing heat pump performance when combined with renewable energy requires moving beyond traditional control strategies. Traditional heat pump controllers, which usually rely on a heating curve, fail to consider factors like solar radiation and internal gain (Rolando and Madani, 2013). Complex systems, such as heat pump systems with different sources can benefit from advanced methods of predictive control (Parisio et al., 2020). In addition, strategies such as MPC can account for variable electricity prices. This offers residential customers the opportunity to reduce costs by scheduling operations during periods of lower electricity prices.

### 1.1 Solar-assisted heat pump system

Heating, Ventilation, and Air Conditioning (HVAC) systems play a critical role in indoor comfort and energy efficiency. The integration of renewable energy sources with conventional systems, such as solar-assisted heat pump (SAHP) systems, has gained attention for its ability to utilize sustainable energy sources (Sezen and Gungor, 2023), improve system efficiency (Hengel et al., 2020), and support the transition to greener technologies. An effective control strategy is essential to optimize efficiency, reduce operating costs, and minimize the environmental footprint, especially in the SAHP system (Perella et al., 2024). In this context, MPC, the focus of this paper, has emerged as a promising approach to optimizing the performance of HVAC systems. The primary objectives of MPC have traditionally included minimizing energy consumption, maximizing comfort, and reducing energy expenses. These goals have been achieved through various methods such as optimal operation with storage systems, implementation of zone temperature control, and optimal


Selection and/or peer review under responsibility of Scientific Committee
10.18086/eurosun.2024.01.06 Available at http://proceedings.ises.org

operation of heat pumps, among others (Drgoňa et al., 2020; Afram and Janabi-Sharifi, 2017; Frison et al., 2019).

### 1.2 Related work

In Multi-Source Heat Pumps (MSHP) systems, supervisory controllers fall into two main categories: MPC and RBC (Pean and Costa-Castello, 2008). These controllers regulate MSHP operation by setting parameters based on factors like solar irradiance, temperatures, and energy storage. RBC, though more advanced than traditional heating curves, lacks MPC's clear objective formulation (Pean and Costa-Castello, 2008) and can become complex with increasing system components. MPC is attractive in HVAC systems for its ability to integrate predictive data from renewable sources and model dynamics, thus improving energy efficiency (Serale et al., 2018). The concept of optimal control for SAHP systems dates to the 1980s (Molyet et al., 2020). Fiorentini et al. (2015) investigated a similar system with PVT collectors, a PCM storage tank, and a heat pump, using Hierarchical Model Predictive Control (HMPC) with a suboptimal two-level control scheme: a high-level controller for a 24-hour horizon and a low-level controller for 1-hour intervals, which may not always yield optimal performance. Hierarchical control strategies are often used in HVAC systems to simplify complex problem formulations and handle nonlinearities, splitting the control into a high-level convex problem and a low-level heuristic-based problem. Switched dynamics in MSHP systems lead to challenging Mixed-Integer Nonlinear Programming (MINLP) formulations, which are managed through techniques like convexification and linearization, transforming problems into Mixed-Integer Linear Programming (MILP) formulations (Atam and Helsen, 2015). Derivative-free methods such as Genetic Algorithms (GA) (Xia et al., 2018) and Particle Swarm Optimization (PSO) (Beghi et al., 2013) are also used. However, GA may yield suboptimal performance if mode selection relies on heuristics rather than being optimally chosen. This work focuses on addressing MINLP problems in MSHP systems, utilizing the Combinatorial Integral Approximation (CIA) technique, previously applied to solar thermal systems (Bürger et al., 2021) and heating networks (Frison et al., 2024).

### 1.3 Contributions

This paper presents a detailed analysis of MPC applied to an advanced solar-assisted MSHP system that integrates PVT collectors, ice storage, a heat pump, and a buffer storage tank. The optimization of this system is complicated by nonlinearities in the model, such as heat transfer interactions between components, hybrid behaviors arising from various operation modes, and the phase change properties of ice storage. These challenges, typically addressed using discrete variables, result in a complex mixed-integer nonlinear optimization problem. To address this, we investigate a real-time control approach using Mixed-Integer Nonlinear MPC (MI-NMPC), offering practical insights into its implementation. Our analysis compares the effectiveness of MPC with an RBC strategy in minimizing energy costs while maintaining indoor comfort. The results reveal that the RBC strategy, as implemented in this study, faces significant difficulties in rule selection and is less effective than MPC.

### 1.4 Paper outline

In this paper, we first outline the heating system description, followed by a mathematical model describing each component and the interactions between them. Section 3 provides a detailed MPC formulation and our solution to the arising optimal control problem. Next, in Section 4, we present and discuss the results obtained from simulations.

## 2. Model development

This section begins with a brief description of the system, followed by a detailed mathematical description of the system model, which is essential for developing the control strategy. The system under consideration is modeled using state-space representation, a method that effectively captures its dynamics.

### 2.1 System description

Figure 1. shows a simplified schematic of an elaborate heating system that integrates photovoltaic thermal (PVT) collectors, an ice storage tank, a heat pump, and a buffer storage tank. At the core of this system is a brine/water heat pump with a rated thermal capacity of 12.1 kW (B0W35, with a 0°C brine source and a 35°C

sink). This heat pump consists of four main components: the evaporator, which absorbs heat from the source fluid; the condenser, which transfers the absorbed heat to the buffer tank; the compressor, which pumps the refrigerant through the system; and the expansion valve, which regulates the refrigerant flow. On the left side of the heat pump, referred to as the source side, the evaporator is connected to PVT collectors and an ice storage tank. The PVT collectors capture solar energy and convert it into thermal and electrical energy. The ice storage tank stores thermal energy. In this work the ice storage is buried underground, and it is not insulated. Thus, it can gain heat from the ground or lose heat to the ground. The ice fraction in the ice storage cannot exceed 70% in this study. The source side of the heat pump system operates in four different modes, visually illustrated in Figure 2. In Mode 1, solely the ice storage serves as the heat source for the evaporator, with brine circulating between them. Conversely, Mode 2 activates only the PVT collectors, directing brine circulation between the collectors and the evaporator. The Parallel mode (Mode 3) combines both sources, efficiently delivering heat to the refrigerant. Lastly, Mode 4 involves the regeneration of the ice storage tank by the PVT collectors during periods when the heat pump is inactive. These modes provide versatility in managing heat sources for optimal system performance. On the right side of the heat pump, called the sink side, the condenser exchanges heat with the buffer tank, which provides heat to the house. The buffer tank plays a crucial role in storing and regulating the heat delivered to the house. The heating system in the house, which includes radiators, uses hot water from the buffer tank to provide consistent and efficient heating. In cases where the heat pump is unable to generate enough heat to reach the set flow temperature of the heating circuit, the auxiliary heating system is activated to provide the required heat.

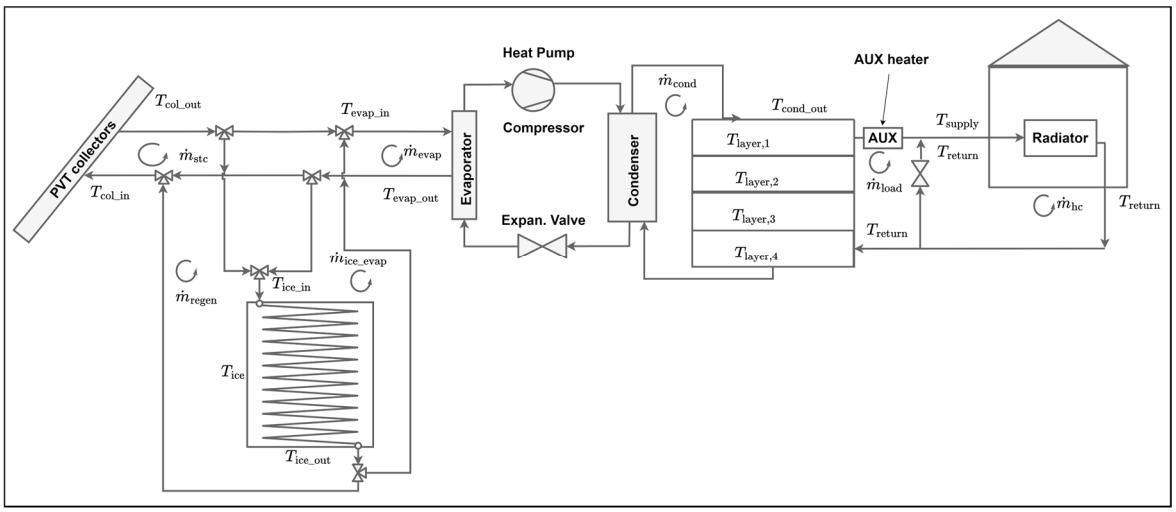


**Fig. 1: Simplified scheme of the system**

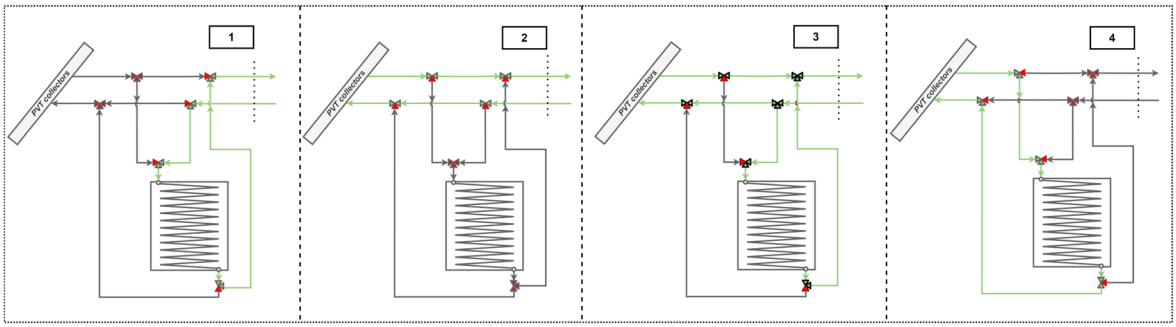


**Fig. 2: Operating modes of the source side of the system**

## 2.2 System model

The system under consideration is modeled using a state space representation. This approach captures the dynamics of the system through differential equations that describe the temperatures at different levels of the system components. The state variables listed in Table 1, are critical for describing the thermal dynamics of the system. The differential equations governing the system states are derived from energy balance principles

applied to the system components.

**Tab. 1 Notation of state variables**

| Symbol | Description | Bounds |
|---|---|---|
| $T_{\text{col\_out}}$ | Temperature of the brine leaving the PVT collectors | [-15, ∞],( °C) |
| $T_{\text{ice}}$ | The heat stored in the ice storage | [-∞, 15],( °C) |
| $T_{\text{ice\_out}}$ | The ice storage hex outlet source fluid temperature | [-∞,∞],( °C) |
| $T_{\text{layer,i}}$ | The temperature of layer *i* in the buffer storage tank | [0,80],( °C) |

Besides the state variables, the system model includes control variables (see Table 2.), disturbances or time-varying parameters (see Table 3.) and finally in Table 4. the model parameters (constants) are given. The control variables can be divided into discrete ones, which describe the modes of the source side, and continuous ones, which describe the power consumption of the compressor and the auxiliary heater.

**Tab. 2 Notation of control variables**

| Symbol | Type | Description | Bounds |
|---|---|---|---|
| $P_{\text{el\_comp}}$ | Continous | Compressor electrical power consumption | [0, 6000],(W) |
| $P_{\text{aux}}$ | Continous | Auxilary heater electrical power consumption | [0, 6000],(W) |
| $b_{\text{i}}$ | Binary | Binary variable for mode i ∈ {1,2,3,4} | {0,1},(-) |

**Tab. 3 Notation of time-varying parameters**

| Symbol | Description |
|---|---|
| $T_{\text{amb}}$ | The ambient temperature ( °C) |
| $T_{\text{supply}}$ | The supply temperature of the heating circuit ( °C) |
| $T_{\text{return}}$ | The return temperature of the heating circuit ( °C) |
| $G_{\text{tot}}$ | Solar irradiance (W/$m^2$) |
| $C_{\text{el}}$ | The price of electricity from the grid (EUR/W$\Delta t$) |
| $\dot{Q}_{\text{load}}$ | The thermal load of the building (W) |

**Tab. 4 Notation constant parameters**

| Symbol | Description | Value | Unit |
|---|---|---|---|
| $c_{\text{eff}}$ | Effective thermal capacity of PVT collectors | 7879 | J/(m $^2$ · K) |
| $h_{\text{hx}}$ | Heat transfer coefficient of heat exchanger | 80 | W/(m $^2$ · K) |
| $A_{\text{hx}}$ | Heat exchange area of hex | 30 | m $^2$ |
| $U_{\text{ice\_storage}}$ | Heat transfer coefficient of the ice tank walls to the ground | 4 | W/(m $^2$ · K) |
| $\rho_{\text{ice}}$ | Density of ice | 920 | kg/m $^3$ |
| $\rho_{\text{w}}$ | Density of water | 1000 | kg/m $^3$ |
| $L_{\text{ice}}$ | The latent heat of fusion for ice | 335 | kJ/kg |
| $T_{\text{amb\_ice}}$ | Surroundings temperature (ice tank) | 5 | °C |
| $\dot{m}_{\text{regen}}$ | Mass flow rate during regeneration mode | 0.35 | kg/s |
| $\dot{m}_{\text{evap}}$ | Evaporator mass flow | 1 | kg/s |
| $\dot{m}_{\text{stc}}$ | Mass flow at PVT collectors | 1 | kg/s |
| $\dot{m}_{\text{ice\_evap}}$ | Mass flow rate at ice storage | 1 | kg/s |
| $\dot{m}_{\text{combined}}$ | Mass flow rate during combined mode | 0.5 | kg/s |
| $R_{\text{ice}}$, $V_{\text{ice}}$ | The radius and volume of tank (ice storage) | 1, 5.2 | m, m $^3$ |
| $c_{\text{br}}$ | Brine specific heat capacity | 3595 | J/kg/K |
| $c_{\text{w}}$ | Water specific heat capacity | 4181 | J/kg/K |
| $\rho_{\text{br}}$ | Brine density | 1000 | kg/m $^3$ |
| $A_{\text{pvt}}$ | PVT collector area | 40 | m $^2$ |
| $V_{\text{buffer}}$ | Volume of tank (buffer storage) | 1 | m $^3$ |
| $l_{\text{buffer}}$ | Height of tank (buffer tank) | 1 | m |
| $T_{\text{amb\_buffer}}$ | Surroundings temperature (buffer tank) | 20 | °C |
| $h_{\text{buffer}}$ | Heat transfer coefficient (buffer tank walls) | 0.4 | W/(m $^2$ · K) |

We have developed a control-oriented model that represents the dynamics of the multisource heat pump system. This model includes equations for the heat pump, PVT collectors, ice storage tank, and buffer tank.

For the thermal part of a PVT system, the energy balance on the absorber plate is given by:

$$\frac{\mathrm{d}}{\mathrm{dt}}T_{\mathrm{col\_out}}(t) = \frac{1}{C_{\mathrm{stc}}}(\dot{Q}_{\mathrm{col}}(t) - b_2(t)\dot{m}_{\mathrm{stc}}c_{\mathrm{br}}(T_{\mathrm{col\_out}}(t) - T_{\mathrm{evap\_out}}(t)) - b_3(t)\dot{m}_{\mathrm{combined}}c_{\mathrm{br}}(T_{\mathrm{col\_out}}(t) - T_{\mathrm{evap\_out}}(t)) - b_4(t)\dot{m}_{\mathrm{regen}}c_{\mathrm{br}}(T_{\mathrm{col\_out}}(t) - T_{\mathrm{ice\_out}}(t))) \quad \text{(eq. 1)}$$

Where $C_{\mathrm{stc}} = c_{\mathrm{eff}}A_{\mathrm{pvt}}$ and $\dot{Q}_{\mathrm{col}}$ is the total heat gain:

$$\dot{Q}_{\mathrm{col}} = \eta_{\mathrm{col}}A_{\mathrm{pvt}}G_{\mathrm{tot}} \quad \text{(eq. 2)}$$

Here $\eta_{\mathrm{col}}$ is the efficiency of collector, which for a flat plate collector can be approximated by the polynomial:

$$\eta_{col} = \alpha_1 - \alpha_2\frac{T_{\mathrm{col\_out}} - T_{\mathrm{amb}}}{G_{\mathrm{tot}}} - \alpha_3\frac{(T_{\mathrm{col\_out}} - T_{\mathrm{amb}})^2}{G_{\mathrm{tot}}} \quad \text{(eq 3)}$$

where $\alpha_1, \alpha_2, \alpha_3$ are parameters of solar thermal collector (-), $(\frac{\mathrm{W}}{\mathrm{Km^2}})$, $(\frac{\mathrm{W}}{\mathrm{K^2m^2}})$.

The electrical power generated by the PV system is:

$$P_{\mathrm{pv\_gen}} = \eta_{\mathrm{pv}}A_{\mathrm{pvt}}G_{\mathrm{tot}} \quad \text{(eq. 4)}$$

The electrical efficiency of the PV panel calculated using the following equation (Zondag et al., 2003):

$$\eta_{\mathrm{pv}} = \eta_0 \cdot (1 - 0.0045(T_{\mathrm{cell}} - T_{\mathrm{ref}})) \quad \text{(eq. 5)}$$

where $\eta_0$ electrical the efficiency of pv at reference temperature $T_{\mathrm{ref}}$ = 25 °C, $T_{\mathrm{cell}}$ is the temperature of the solar cell.

For the ice storage model, we first define the ice fraction as a sigmoid function:

$$f = \frac{1}{(1 + e^{2(T_{ice} - Tm)})} \quad \text{(eq. 6)}$$

The energy balance equation for the ice storage is:

$$\frac{\mathrm{d}}{\mathrm{dt}}T_{\mathrm{ice}}(t) = \frac{1}{m_{\mathrm{ice}}\left(c_{\mathrm{p}} + L_{\mathrm{ice}}\frac{\mathrm{d}f(T)}{\mathrm{d}T}\right)}(b_4(t)c_{\mathrm{br}}\dot{m}_{\mathrm{regen}}(T_{\mathrm{col\_out}}(t) - T_{\mathrm{ice\_out}}(t)) - b_1(t)c_{\mathrm{br}}\dot{m}_{\mathrm{ice\_evap}}(T_{\mathrm{ice\_out}}(t) - T_{\mathrm{evap\_out}}(t)) - b_3(t)c_{\mathrm{br}}\dot{m}_{\mathrm{combined}}(T_{\mathrm{ice\_out}}(t) - T_{\mathrm{evap\_out}}(t)) - UA_{\mathrm{ice\_storage}}(T_{\mathrm{ice}}(t) - T_{\mathrm{amb\_ice}})) \quad \text{(eq. 7)}$$

To determine the output temperature of the fluid in a heat exchanger immersed in the ice storage system, the energy balance is applied. The rate of change of the brine outlet temperature can be expressed as:

$$\frac{\mathrm{d}}{\mathrm{dt}}T_{\mathrm{ice\_out}}(t) = \frac{1}{V_{\mathrm{hx}}}(b_1(t)\left(\frac{\dot{m}_{\mathrm{ice\_evap}}}{\rho_{\mathrm{br}}}(T_{\mathrm{evap\_out}}(t) - T_{\mathrm{ice\_out}}(t)) - \frac{\dot{Q}_{\mathrm{net,1}}}{\rho_{\mathrm{br}}c_{\mathrm{br}}}\right) + b_3(t)\left(\frac{\dot{m}_{\mathrm{combined}}}{\rho_{\mathrm{br}}}(T_{\mathrm{evap\_out}}(t) - T_{\mathrm{ice\_out}}(t)) - \frac{\dot{Q}_{\mathrm{net,3}}}{\rho_{\mathrm{br}}\cdot c_{\mathrm{br}}}\right) + b_4(t)\left(\frac{\dot{m}_{\mathrm{regen}}}{\rho_{\mathrm{br}}}(T_{\mathrm{col\_out}}(t) - T_{\mathrm{ice\_out}}(t)) - \frac{\dot{Q}_{\mathrm{net,4}}}{\rho_{\mathrm{br}}\cdot c_{\mathrm{br}}}\right)) \quad \text{(eq. 8)}$$

Then $\dot{Q}_{\mathrm{net,i}}$ is given as follows:

$$\dot{Q}_{\mathrm{net,i}} = U_{\mathrm{hx}}A_{\mathrm{hx}}\Delta T_{\mathrm{MTD,i}}\text{ , where } i \text{ refers to the mode of operation, and } \Delta T_{\mathrm{MTD,i}} \text{ is given as a mix of geometric and arithmetic mean temperatures .} \quad \text{(eq. 9)}$$

The buffer storage tank is modeled as a stratified tank divided into $n$ ($n$=4) layers based on Eicker (2003). From the energy balance equations applied to each layer, the rate of temperature change for each layer is derived. For the intermediate layer $i$, it is given as:

$$\frac{\mathrm{d}}{\mathrm{dt}}T_{\mathrm{layer,i}} = \frac{1}{m_{\mathrm{layer,i}}c_{\mathrm{w}}}\begin{pmatrix} -UA_{\mathrm{lat}}\left(T_{\mathrm{layer,i}} - T_{\mathrm{amb}}\right) - UA_{\mathrm{layer}}\left(T_{\mathrm{layer,i}} - T_{\mathrm{layer,i+1}}\right) \\ +UA_{\mathrm{layer}}\left(T_{\mathrm{layer,i-1}} - T_{\mathrm{layer,i}}\right) \\ +\dot{m}_{\mathrm{cond}} \cdot c_{\mathrm{w}}\left(T_{\mathrm{layer,i-1}} - T_{\mathrm{layer,i}}\right) - \dot{m}_{\mathrm{load}}c_{\mathrm{w}} \cdot \left(T_{\mathrm{layer,i}} - T_{\mathrm{i+1}}\right) \end{pmatrix} \quad \text{(eq. 10)}$$

Here $UA_{\mathrm{lat}}$, $UA_{\mathrm{layer}}$ represent the overall transfer coefficients for lateral-to-ambient transfer and transfer between layers, respectively and $m_{\mathrm{layer,i}}$ represents the mass of each layer.

In total, Equations (1), (7), (8), (10), and three equations for the remaining layers based on Equation (10) are the differential equations describing the evolution of the system's states. In these equations, the thermal power output of the heat pump is defined by:

$$\dot{Q}_{\mathrm{th\_cond}}(t) = P_{\mathrm{el\_comp}}(t)(b_1(t) \cdot \mathrm{COP}_1(t) + b_2(t) \cdot \mathrm{COP}_2(t) + b_3(t) \cdot \mathrm{COP}_3(t)) \quad \text{(eq. 11)}$$

For each mode $COP_i$ ($i$ corresponding to mode $i \in \{1,2,3\}$), it is defined by a function with corresponding inlet temperature of evaporator and temperature at sink side This approach avoids double multiplication of the binary control variable, so only the outer multiplication of a binary variable is carried out. The condenser mass flow is calculated by:

$$\dot{m}_{\mathrm{cond}}(t) = \frac{\dot{Q}_{\mathrm{th\_cond}}(t)}{c_{\mathrm{w}}(\Delta T_{\mathrm{condenser}}(t))} \quad \text{(eq. 11)}$$

We assume a constant temperature difference between the inflow and outflow from the condenser:

$$\Delta T_{\mathrm{condenser}}(t) = T_{\mathrm{cond\_out}}(t) - T_{\mathrm{layer,4}}(t) = 5 \quad \text{(eq. 12)}$$

In this paper, COP and the maximum thermal output of the heat pump are estimated using a polynomial function that depends on the temperatures of the source and sink sides.

## 2.3 Assumptions

To simplify the system model for optimization, several key assumptions were made. First, mass flow rates are assumed to be constant across all operational modes, which reduces the number of dynamic variables in the system. Additionally, the power of the compressor is treated as a continuous variable, avoiding the complexities associated with discrete power levels. Concerning the sink side, a constant temperature difference is assumed, and heat losses to the environment from both the evaporator and condenser are considered negligible. Ambient temperature around the ice storage and buffer tanks is also assumed to be constant, which simplifies the boundary conditions. Furthermore, the densities and viscosities of the brine and water are treated as constant, eliminating the need to account for temperature-dependent variations. The model maintains mass balance by ensuring that the mass flow rates entering and exiting each control volume are equal. Lastly, both the source and sink fluids are considered incompressible, which simplifies the fluid dynamics equations.

## 2.4 Boundary conditions

In terms of MPC, the boundary conditions are given in the form of a disturbance vector, which partially includes calculated variables. In our case, ambient temperature, solar irradiance, and the price of electricity are predicted variables, while the heating demand, supply, and return temperatures of the heating circuit are calculated. The predicted variables are provided for the simulated period. For simulation purposes, dynamic pricing is used, with data obtained from the European Energy Exchange (EEX), visually shown in Figure 3. The calculated variables in the disturbance vector are derived using the house parameters and the predicted variables.

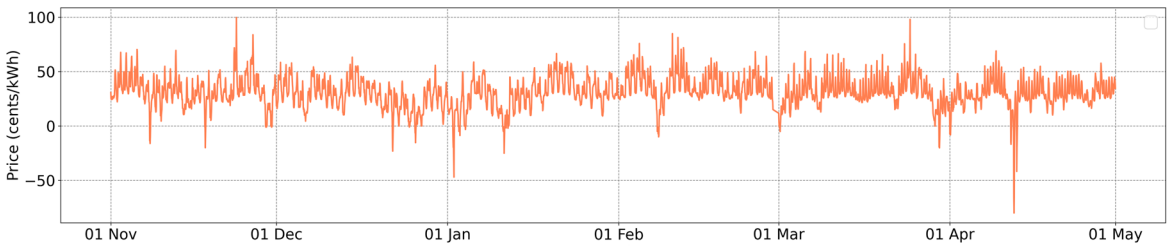


**Fig. 3: The price of the electricity used in the simulations**

Since the current project develops the control strategy for a house in Ulm, Germany, the house parameters and

the disturbance vector are specific to this house and location. The calculated variables represent the operating parameters of a heating system designed to maintain a comfortable indoor environment. This includes maintaining an indoor temperature of 20°C. At a nominal outdoor temperature of -13°C, the heating system should provide heat to the house, and have a supply (flow) temperature of 45°C and a return temperature to the heat exchangers (radiators) of 35°C. These calculations are performed for the actual house with the goal of developing a cost- and energy-efficient control strategy. By integrating the predicted variables with the house parameters, the control strategy aims to optimize the performance of the heating system while minimizing energy consumption and costs.

## 3. Model predictive control formulation

Model Predictive Control (MPC) is a widely used optimization-based control strategy in process engineering. This approach uses a mathematical model of the controlled system to predict its future behavior over a finite time horizon, known as the prediction horizon. In our system, the mathematical model is defined by the differential equations described in the previous section. MPC solves an optimization problem to determine the optimal trajectory of the system states, producing control inputs that meet the desired objectives while satisfying the constraints. MPC considers future disturbances, such as weather conditions, demand and electricity prices, as detailed in the previous section. Predictions of these disturbances are provided for this study. For more realistic results, the control data from the optimization is applied on the system with disturbances, including random noise. This approach introduces discrepancies between the model and the actual system to better capture real world scenarios.

### 3.1 Optimal control problem formulation

Given the previously defined states $x \in \mathbb{R}^{n_x}$ ($n_x = 7$) as described in Table 1, and the differential equations are given in the previous section, the OCP is formulated. The controls include continuous variables $u \in \mathbb{R}^{n_u}$ ($n_u = 2$) and binary variables $b \in \mathbb{R}^{n_b}$ ($n_b = 4$), time-varying parameters $p \in \mathbb{R}^{n_p}$ ($n_p = 6$), and slack variables $s \in \mathbb{R}^{n_s}$ ($n_s = 1$). The objective function aims to minimize the cost of electricity consumed, maximize the utilization of solar energy, and minimize the use of the auxiliary heating system (see Equation 13, where $W_i$ is a weighting coefficient for each component of the objective function). Additionally, it includes quadratic penalty terms for the slack variables. Constraints are then defined, leading to the formulation of the OCP.

$$\min J = \int_0^{tf} \sum_{i=1}^{4} b_{\mathrm{i}}(t) \left( W_{\mathrm{el}} \cdot C_{\mathrm{el}}(t) \cdot P_{\mathrm{el,comp}}(t) - W_{\mathrm{el},2} P_{\mathrm{el,comp}}(t) G_{tot}(t) \right) + W_{\mathrm{aux}} P_{\mathrm{aux}}(t) + W_{\mathrm{s,q}} s^2(t) dt \quad \text{(eq. 13)}$$

s.t.

$$x(t_0) = x_0 \quad \text{(eq. 14)}$$

$$\dot{x}(t) = f(x(t), u(t), p(t)) + \sum_{i=1}^{4} b_i(t) f_b(x(t), u(t), p(t)) \quad \text{(eq. 15)}$$

$$\sum_{i=1}^{4} b_{\mathrm{i}}(t) \leq 1 \quad \text{(eq. 16)}$$

$$T_{\mathrm{hc\_supply}}(t) \leq T_{\mathrm{layer},1}(t) + s(t) \quad \text{(eq. 17)}$$

$$P_{\mathrm{el\_comp}}(t) COP(t) \leq Q_{\mathrm{th,max}}(t) \quad \text{(eq. 18)}$$

$$P_{\mathrm{el\_comp,MIN}} \sum_{i=1}^{3} b_i(t) \leq P_{\mathrm{el\_comp}}(t) \quad \text{(eq. 19)}$$

$$P_{\mathrm{el\_comp}}(t) \leq \sum_{i=1}^{3} b_{\mathrm{i}}(t) M \quad \text{(eq. 20)}$$

$$P_{\mathrm{el\_comp}}(t) \leq (1 - b_4(t)) M \quad \text{(eq. 21)}$$

$$x(t) \in [x_{\mathrm{lb}}, x_{\mathrm{ub}}]^{n_{\mathrm{x}}} \quad \text{(eq. 22)}$$

$$u(t) \in [u_{\mathrm{lb}}, u_{\mathrm{ub}}]^{n_{\mathrm{u}}} \quad \text{(eq. 23)}$$

$$b(t) \in \{0,1\}^{n_{\mathrm{b}}} \quad \text{(eq. 24)}$$

Eq. (14) ensures that the system starts from a specified initial state. The system's evolution is described by the differential equations in Eq. (15). The binary constraint in Eq. (16) guarantees that only one mode is active at any given time. Eq. (17) involves the tank temperature and supply temperature to consistently meet the house's heat demand. By introducing a slack variable, this constraint is relaxed, allowing for more solver flexibility, though it results in a minor negative temperature deviation, which is penalized in the objective function. Eq. (18) pertains to heat pump operation, stating that the electric power consumed by the heat pump, multiplied by

the COP, cannot exceed the maximum possible thermal power output. Eq. (19) defines the minimum input of the heat pump in terms of the electric power of the compressor, which is active in one of the operational modes when the heat pump is on. Conversely, Eq. (20) ensures that when the heat pump is off, its electric power input is zero. Finally, Eq. (21) ensures that when the regeneration mode is active, the electric input to the compressor is zero. In these equations, *M* refers to the Big M method. Eqs. (22, 23, and 24) constrain the lower and upper bounds for the state variables, continuous control variables, and binary control variables, respectively.

### 3.2 Solution approach

The following is the methodology used to solve the Optimal Control Problem (OCP) described in Eqs. (13-24). The OCP includes both continuous and discrete control variables, where the discrete variables are binary. This results in a Mixed Integer Optimal Control Problem (MIOCP). To solve the continuous-time OCP, the problem is discretized using the direct collocation method, which converts the infinite-dimensional optimization problem into a Mixed-Integer Nonlinear Programming (MINLP) problem. While solvers such as BONMIN (Bonami et al., 2008) can handle MINLP problems, they are often impractical for real-world applications due to their long computation times and the need to satisfy real-time constraints, especially when dealing with large problems at each time step. In this study, the Combinatorial Integral Approximation (CIA) technique, as described by Sager et al. (2011) and practically demonstrated by Bürger et al. (2021), is employed. This algorithm consists of three main steps, which are outlined in Algorithm 1.

**Algo. 1 Algorithm for Solving the MIOCP**

| |
|---|
| 1. Solve the relaxed discretized MIOCP (MINLP) with $b_i \in [0, 1]$ |
| 2. Solve the CIA problem to obtain $b_i \in \{0, 1\}$ |
| 3. Solve the discretized MIOCP (MINLP) with $b_i \in \{0, 1\}$ |
| Output: *x, u, b* |

In the closed loop simulation, the obtained control variables are applied to the system after step 3 in Algorithm 1. The system is simulated using the fourth-order Runge-Kutta (RK4) integration scheme. To improve computational efficiency, warmstarting is used to transfer solution information from the previous MIOCP problem to the current one as an initial guess. According to Rawlings et al. (2017), shift initialization is particularly beneficial for systems with time-varying parameters in their dynamics. In this technique, the solution of the previous MINLP problem is shifted to the next one and adapted to the next time step. We apply the shift initialization technique specifically to the relaxed MIOCP problem.

All the computations were carried out on a desktop PC equipped with an Intel(R) Core(TM) i5-9500 @ 3.00 GHz CPU and 16 GB of RAM, running on the Windows 10 operating system. The CasADi symbolic framework (version 3.6.3) (Andersson et al., 2019), which provides algorithmic differentiation capabilities, was used to formulate and solve the (MIOCP) problems. IPOPT (3.14.11) (Wächter and. Biegler, 2006) has been used for solving the sparse NLP problems using the linear solver MUMPS (5.4.1.) (Amestroy et al., 2001). For solving the CIA (Sager et al., 2011) problems, the open-source package pycombina (Bürger et al., 2020) was used, with MILPs solved using the branch-and-bound algorithm. All code was written in Python.

## 4. Results

### 4.1 Overview of controllers

To evaluate the performance of the MI-NMPC strategy, a reference control strategy was needed. This work included the implementation of the RBC strategy, which is based on simple heuristics. These heuristics were partially derived from observations of the MI-NMPC simulation. The RBC strategy utilizes solar energy when it is available.

### 4.2 Case study: Heating season simulation

This section presents and analyzes the outcomes of closed-loop simulations comparing the MI-NMPC strategy to the RBC strategy for the heating heat pump system during a heating season. A sampling time for MI-NMPC is $\Delta T = 900$ seconds, and RBC inputs are updated every 900 seconds. To begin with, there is a notable disparity in the utilization of the auxiliary heater when comparing RBC and MI-NMPC control strategies. Specifically,

the MI-NMPC strategy reduces auxiliary heater usage by a factor of 4.3, compared to RBC. In percentage terms, the auxiliary heater accounts for 4.3% of the total heat delivered when the system is controlled by the RBC strategy, versus only 1% with MI-NMPC.

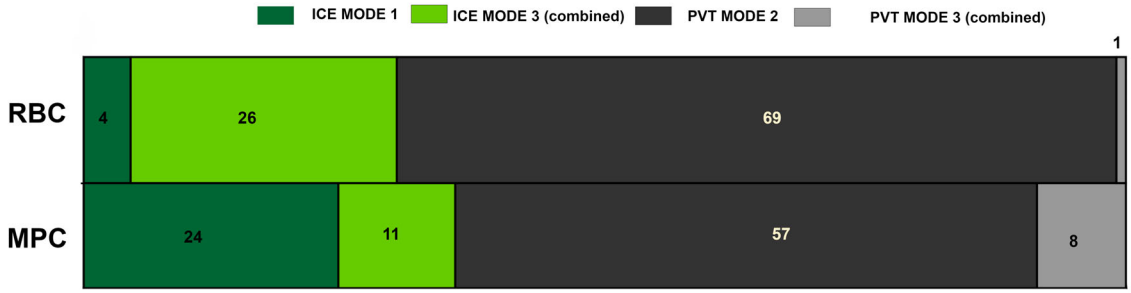


**Fig. 4: Heat flow (in percent, %) from PVT and ice storage in each mode**

Next, Figure 4. demonstrates the amount of heat delivered to the evaporator from each source and during each mode when controlled by MI-NMPC and RBC strategies and Figure 5. shows the ice fraction, temperature inside the ice storage tank, and the thermal power output of the auxiliary heater throughout the simulation period for both MI-NMPC and RBC strategies. The utilization of ice storage is lower for the RBC strategy due to the depletion of ice storage, with the ice fraction achieving its maximum allowed value. In contrast, the MI-NMPC strategy better utilizes ice storage in mode 1, with 24% utilization compared to 4% for RBC. During the combined mode with MI-NMPC, the PVT collectors contributed 8% of the total heat, compared to 1% with RBC over the entire simulation period. In total, solar thermal energy (PVT) accounts for more than 65% of the total heat source for both controllers. This high proportion is likely due to the under sizing of the ice storage system for this application. When the ice storage tank is depleted, both strategies employ the auxiliary heater. However, MI-NMPC reduces utilization to 0.25 MWh compared to 1.08 MWh for RBC. In addition, the economic analysis revealed that with MI-NMPC, the electricity bill is 1776 EUR, with a PV feed-in revenue of 233 EUR, resulting in net expenses of 1543 EUR. In contrast, for RBC, the electricity bill is 2151 EUR, with a PV feed-in revenue of 327 EUR, indicating less PV self-consumption. Economically, MI-NMPC results in net expenses of 15.4% less compared with RBC, further demonstrating its superior cost performance. Figure 7. illustrates the cumulative cost of electricity for both cases over the simulated period. From an energy management perspective, MI-NMPC optimizes the operation of the heat pump, resulting in better energy consumption management and significant cost savings. The utilization of solar energy is notably more effective with MI-NMPC, showcasing a higher self-consumption of generated PV electricity, with 38.2% compared to 34.5% for RBC.

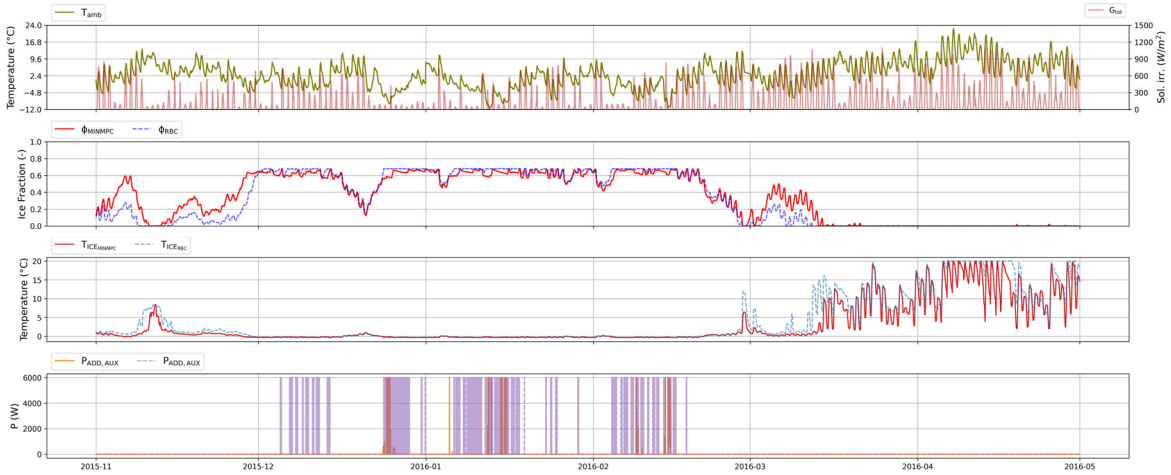


**Fig. 5: Ice fraction, temperature inside ice storage, activation of auxiliary heating system for both MINMPC and RBC controlled cases**

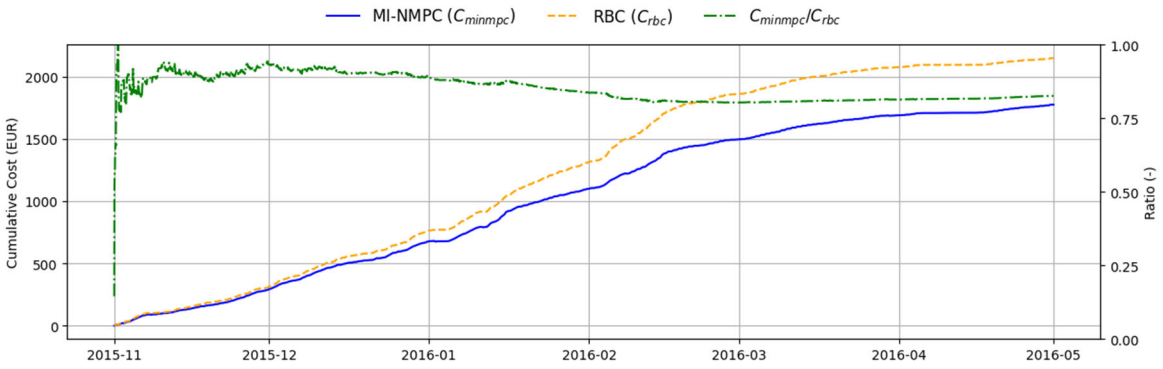


**Fig. 6: Cumulative electricity costs over simulated time**

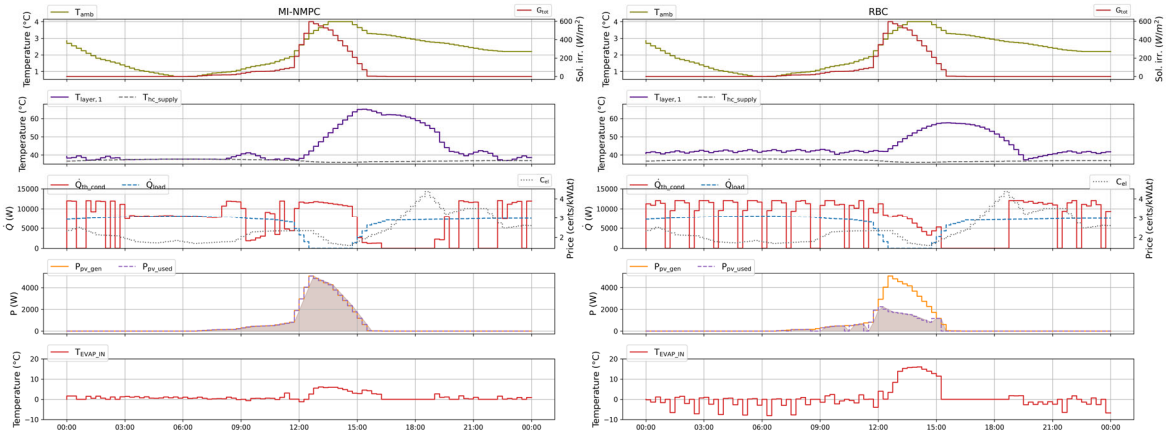


**Fig. 7: Simulation Results: Detailed visualization of key parameters and operational aspects under MI-NMPC (left) and RBC (right) control strategies.**

To provide a detailed analysis, we look at the results of a one-day simulation. While a general overview of the entire heating season was provided, the detailed one-day simulation results offer insights into the specific operational differences of MI-NMPC. The sampling time for MI-NMPC is $\Delta T = 900$ seconds, and RBC inputs are updated every 900 seconds. Figure 8. presents plot of the simulation results from 00:00 to 00:00 the following day for both control strategies, with MI-NMPC on the left and RBC on the right. The first subplot displays changes in temperature and solar irradiance levels over the day, with the average ambient temperature on the selected day above 0°C. The second subplot shows the temperature of the top layer of the tank and the supply temperatures, with both controllers meeting the heating demand. The third subplot illustrates the heat pump's thermal output and demand changes over a 24-hour period, with the electricity price on another y-axis. The fourth subplot demonstrates that MI-NMPC charges the buffer tank when electricity is cheap or PV generation is available, consuming 100% of PV-generated electricity compared to 48.5% with RBC. The last subplot illustrates the input temperatures of the evaporator, with MI-NMPC maintaining higher, steadier temperatures, leading to fewer mode changes compared to RBC.

Several observations can be made based on the simulation results. The MI-NMPC strategy effectively meets heating demand while minimizing electricity costs, dynamically adapting to changing conditions, and optimizing storage utilization. This adaptability shows potential in dynamic pricing scenarios. The study also highlights the benefits of combining expertise from different fields to address complex HVAC and energy management challenges.

## 5. Conclusion

In conclusion, this study confirms the effectiveness of the MI-NMPC strategy in meeting heating demands while minimizing electricity costs. The MI-NMPC strategy significantly reduces auxiliary heater utilization and demonstrates superior economic performance, with electricity costs reduced by up to 17.4% over the entire heating season and net costs lowered by 15.4%, including income from electricity sold back to the grid. Additionally, the MI-NMPC strategy optimizes energy consumption, achieving a higher self-consumption rate

of 38.2% for generated PV electricity. The research contributes to control-oriented modeling and implementation of MI-NMPC strategies and paves the way for future research in MPC for multi-source heat pump systems. Overall, the MI-NMPC strategy shows superior performance in terms of demand satisfaction, cost minimization, and energy efficiency compared to the RBC strategy.

## 6. Acknowledgments

D. Khamidov would like to acknowledge Prof. Dr. Moritz Diehl and Prof. Dr. Hans-Martin Henning for their support and guidance throughout this project. He also extends his gratitude to Fraunhofer ISE and co-authors Dr. L. Frison, B.B. Bampi, and B. Nienborg for the opportunity to work on this project.

The study presented in this paper received funding from the German Federal Ministry of Economic Affairs and Climate Action (BMWK) under the grant agreement number FKZ 03EN4016A (HPPVT40).

## 7. References

Afram, A., Janabi-Sharifi, F., 2017. Supervisory model predictive controller (MPC) for residential HVAC systems: Implementation and experimentation on archetype sustainable house in Toronto. Energy and Buildings, 154, 268-282.

Andersson, J. A. E., Gillis, J., Horn, G., Rawlings, J. B., Diehl, M., 2019. CasADi: a software framework for nonlinear optimization and optimal control. Mathematical Programming Computation, 11(1), 1-36.

Atam, E., Helsen, L., 2015. A convex approach to a class of non-convex building HVAC control problems: Illustration by two case studies. Energy and Buildings, 93, 269-281.

Beghi, A., Cecchinato, L., Rampazzo, M., Simmini, F., 2013. Modeling and control of HVAC systems with ice cold thermal energy storage. In 52nd IEEE Conference on Decision and Control, pp. 4808-4813.

Bonami, P., Biegler, L.T., Conn, A.R., Cornuéjols, G., Grossmann, I.E., Laird, C.D., Lee, J., Lodi, A., Margot, F., Sawaya, N., Wächter, A., 2008. An algorithmic framework for convex mixed integer nonlinear programs. Discrete Optimization, 5(2), pp.186-204.

Bürger, A., Bull, D., Sawant, P., Bohlayer, M., Klotz, A., Beschütz, D., Altmann-Dieses, A., Braun, M., Diehl, M., 2021. Experimental operation of a solar-driven climate system with thermal energy storages using mixed-integer nonlinear model predictive control. Optimal Control Applications and Methods, 42(5), 1293-1319.

Bürger, A., Zeile, C., Hahn, M., Altmann-Dieses, A., Sager, S., Diehl, M., 2020. pycombina: An open-source tool for solving combinatorial approximation problems arising in mixed-integer optimal control. IFAC-PapersOnLine, 53(2), 6502-6508.

Bundesverband der Deutschen Heizungsindustrie (BDH), 2024. Pressemitteilung: Heizungsindustrie: Rekordabsatz in turbulentem Marktumfeld. Available online: https://www.bdh-industrie.de/fileadmin/user_upload/Pressemeldungen/PM_BDH_Jahresbilanz_Gesamtmarkt_19022024.pdf [Accessed: 11 August 2024].

Drgoňa, J., Arroyo, J., Cupeiro Figueroa, I., Blum, D., Arendt, K., Kim, D., Ollé, E.P., Oravec, J., Wetter, M., Vrabie, D.L., Helsen, L., 2020. All you need to know about model predictive control for buildings. Annual Reviews in Control, 50, 190-232.

Eicker, U., 2003. Solar Technologies for Buildings. Chichester: John Wiley & Sons Ltd.

Federal Association of the German Heating Industry, 2024. Available online: https://www.bmwsb.bund.de [last accessed: 07 August 2024].

Fiorentini, M., Cooper, P., Ma, Z., Robinson, D.A., 2015. Hybrid model predictive control of a residential HVAC system with PVT energy generation and PCM thermal storage. Energy Procedia, 83, 21-30.

Frison, L., Kleinstück, M., Engelmann, P., 2019. Model-predictive control for testing energy flexible heat pump operation within a Hardware-in-the-Loop setting. Journal of Physics: Conference Series, 1343(1), 012068.

Frison, L., Kollmar, M., Oliva, A., Bürger, A., Diehl, M., 2024. Model predictive control of bidirectional heat transfer in prosumer-based solar district heating networks. Applied Energy, 358, 122617. https://doi.org/10.1016/j.apenergy.2023.122617.

Hengel, F., Heschl, C., Inschlag, F., Klanatsky, P., 2020. System efficiency of PVT collector driven heat pumps. International Journal of Thermofluids, 5-6, 100034.

International Energy Agency, 2023. Tracking clean energy progress 2023. Available online: https://www.iea.org/reports/tracking-clean-energy-progress-2023. Licence: CC BY 4.0.

Molyet, R.G., Eltimsahy, A.H., Jones, M.L., 1980. Optimal control of solar heating systems utilizing a dual source heat pump. Proc. Annu. Meet. - Am. Sect. Int. Sol. Energy Soc.; (United States).

Parisio, A., Fabietti, L., Molinari, M., Varagnolo, D., Johansson, K.H., 2014. Control of HVAC systems via scenario-based explicit MPC. In 53rd IEEE Conference on Decision and Control, pp. 5201-5207.

Pean, T.Q., Salom, J., Costa-Castello, R., 2019. Review of control strategies for improving the energy flexibility provided by heat pump systems in buildings. Journal of Process Control, 74, 35-49.

Perrella, S., Bisegna, F., Bevilacqua, P., Cirone, D., Bruno, R., 2024. Solar-assisted heat pump with electric and thermal storage: The role of appropriate control strategies for the exploitation of the solar source. Buildings, 14(1).

Rawlings, J.B., Mayne, D.Q., Diehl, M., 2017. Model Predictive Control: Theory, Computation, and Design (2nd ed.). Nob Hill Publishing.

Rolando, D., Madani, H., 2018. Smart control strategies for heat pump systems. Available online: https://varmtochkallt.se/wp-content/uploads/Projekt/EffsysExpand/P18_Project_Report_final_reviewed.pdf [Accessed: 8 August 2024].

Sager, S., Jung, M., Kirches, C., 2011. Combinatorial integral approximation. Mathematical Methods of Operations Research, 73, 363-380.

Sezen, K., Gungor, A., 2023. Comparison of solar assisted heat pump systems for heating residences: A review. Solar Energy, 249, 424-445.

Serale, G., Fiorentini, M., Capozzoli, A., Bernardini, D., Bemporad, A., 2018. Model predictive control (MPC) for enhancing building and HVAC system energy efficiency: Problem formulation, applications and opportunities. Energies, 11, 631.

Umweltbundesamt, 2023. Modernisierungsmaßnahmen zur Emissionsreduktion. Available online: https://www.umweltbundesamt.de/emissionsreduktion-2023. Licence: CC BY 4.0.

Wächter, A., Biegler, L., 2006. On the implementation of an interior-point filter line-search algorithm for large-scale nonlinear programming. Mathematical Programming, 106, 25-57.

Xia, L., Ma, Z., Kokogiannakis, G., Wang, S., Gong, X., 2018. A model-based optimal control strategy for ground source heat pump systems with integrated solar photovoltaic thermal collectors. Applied Energy, 228, 1399-14

Zondag, H.A., de Vries, D.W., van Helden, W.G.J., van Zolingen, R.J.C., van Steenhoven, A.A., 2003. The yield of different combined PV-thermal collector designs. Solar Energy, 74(3), pp.253-269. https://doi.org/10.1016/S0038-092X(03)00121-X.